Sorption and Pore Condensation Behavior of Nitrogen, Argon, and Krypton in Mesoporous MCM-48 Silica Materials

Matthias Thommes

Quantachrome GmbH, Rudolf Diesel Strasse 12, D-85235 Odelzhausen, Germany

Ralf Köhn and Michael Fröba*

Institute of Inorganic and Applied Chemistry, University of Hamburg, Martin Luther-King Platz 6,
D-20146 Hamburg, Germany

Received: November 22, 1999; In Final Form: June 6, 2000

We present results of a systematic study on the sorption- and phase behavior of nitrogen, argon, and krypton at 77 and 87 K in different pristine mesoporous MCM-48 silica phases (BJH pore diameters 2−3 nm) and MCM-48 silica/iron(III) host compound, which consists of two interwoven, but unconnected three-dimensional pore systems. Different methods (e.g., BET, BJH, SF) were used to analyze nitrogen (77 K) and argon (87 K) sorption isotherms in order to characterize the MCM-48 silica materials with respect to surface area, pore volume and pore diameter. In contrast to nitrogen, argon, and krypton sorption isotherms on all MCM-48 silica materials reveal phase transitions accompanied by sorption hysteresis of type H1 (IUPAC classification) down to temperatures T well below the bulk triple-point temperature T_R, i.e., 87 K ($T_R - T \approx 28.5$ K) in the case of krypton and 77 K ($T_R - T \approx 6.5$ K) in the case of argon. Details of the sorption hysteresis depend on temperature and pore size, e.g., with increasing temperature and decreasing pore size a shrinkage of the hysteresis loops is observed. In contrast to the argon/MCM-48 silica system, argon sorption isotherms at $T_R - T \approx 6.5$ K in controlled-pore glass of BJH pore diameter ca. 16 nm reveal no pore condensation and hysteresis, indicating that in such wide pores the pore condensation line does not extend down to this temperature for pressures up to the corresponding bulk sublimation pressure.

1. Introduction

The discovery of ordered mesoporous molecular sieves (denoted as M41S family)[1,2] has expanded the range of uniform pore sizes from the micropore into the mesopore regime and attracted great attention in different fields of materials science, i.e., catalysis,[3,4] nanostructured host−guest compounds,[5] and sorption materials. Originally, this family has been classified into three subgroups: a hexagonal (MCM-41), a cubic (MCM-48, space group: $Ia\bar{3}d$), and a lamellar phase (MCM-50). All of them will be prepared via an electrostatic templating route using cationic quaternary ammonium micelles (S^+), which act as structure directing agents in order to mesostructure anionic inorganic precursors (I^-). This electrostatic assembly, which is driven by electrostatic and steric interactions at the organic−inorganic interface could be extended to further combinations of ion pairs, including charge-reversed (S^-I^+) and counterion mediated ($S^+X^-I^+$ and $S^-X^+I^-$) synthetic pathways.[6] Instead of charged templates it is also possible to use neutral (S^0)[7] or nonionic surfactant molecules (N^0),[8] which interact with the inorganic building units via weak hydrogen bonds. In contrast, very strong organic−inorganic interactions will be achieved in the so-called ligand-assisted liquid−crystal templating in which covalent bonds are formed between the inorganic precursor species and the organic surfactants prior to the self-assembly process.[9] Recently, it could be shown that appropriate surfactants can even act both: as template as well as reactants in the course of the synthesis.[10] For further information and a more comprehensive description on the variety of different synthetic pathways, we refer at this point to ref 11.

In this study we have focused our work on the cubic MCM-48 phase. The surface-defining MCM-48 is the gyroid or G-surface, forming a structure with the space group $Ia\bar{3}d$,[12−14] which is frequently observed in water−surfactant systems.[15,16] The structure contains a three-dimensional network with channels running along [111] and [100], which provides large surface areas and a high accessibility of sites within the porous network structure even if part of the pore entrances cannot be used due to blockage, which is a great advantage in comparison to the one-dimensional channel system of MCM-41. In comparison to MCM-41, the synthesis of MCM-48 is more difficult, which is the reason why only few groups have focused their efforts on this particular cubic phase in the beginning.[17−21] Due to its special pore structure, the mesoporous MCM-48 phase is very interesting as a matrix to immobilize catalytically active metal species,[22−24] e.g., Ti,[25−30] V,[31,32] Cr,[33] Mn,[34] Al,[35−37] Fe,[38] Cu,[39,40] and Zr,[41] onto or within the silica walls or as a host to accommodate nanostructured guest compounds.[42] In addition to the interest in new catalysts, several studies have been published within the last 3 years, which were devoted to new synthetic pathways in order to optimize the synthesis,[43−47] to obtain single crystals[48] or special morphologies,[49,50] to investigate the formation mechanism,[51,52] as well as to analyze the mechanical stability of MCM-48 type of materials.[53]

In addition to the importance of the M41S materials for size- and shape-selective applications, these materials have been also

---

* Corresponding author. Phone: +49 40 42838 3137. Fax: +49 40 42838 6348. E-mail: froeba@xray.chemie.uni-hamburg.de.

10.1021/jp994133m CCC: $19.00

regarded as suitable mesoporous model adsorbents for testing theoretical predictions of pore condensation and hysteresis**.** The state and thermodynamic stability of pure fluids in narrow pores depends on one hand on the interplay between the strength of fluid−wall and fluid−fluid interactions and the effects of confined pore space on the other. While in micropores (pore width < 2 nm) the sorption behavior is dominated almost entirely by the interactions between fluid molecules and the pore wall, pore-filling phenomena occurring in mesopores (pore width: 2−50 nm) depend both on the attractive fluid−wall and fluid−fluid interactions, which may lead to pore condensation.[54,55]

Pore condensation represents a first-order phase transition from a gas to a liquid-like state of the pore fluid occurring at a pressure p less than the correspondent saturation pressure p_0 of the bulk fluid. In the classical Kelvin equation the occurrence of pore condensation, i.e., the shift of the gas−liquid phase transition of a confined fluid from bulk coexistence, is expressed in macroscopic quantities, such as the surface tension γ of the bulk fluid, the densities of the coexistent liquid ρ^{l} and gas ρ^{g}, and the contact angle θ of the liquid meniscus against the pore wall. For cylindrical pores, the Kelvin equation is given by

$$\ln(p/p_0) = -2\gamma\cos\theta/k_bT\Delta\rho(R_p - t_c) \qquad (1)$$

where $\Delta\rho = \rho^{l} - \rho^{g}$, T = experimental temperature, k_b = Boltzmann constant, R_p the pore radius, and t_c the thickness of an adsorbed mulilayer film at the onset of pore condensation, which is formed prior to pore condensation.[55] The stability of this multilayer film, which covers in the case of complete wetting the pore walls, is determined by the attractive fluid-wall interactions, the surface tension, and curvature of the liquid−vapor interface. In the range of small film thickness, the attractive fluid−wall interactions dominate and multilayer adsorption occurs. When the adsorbed liquid-like film becomes thick, however, curvature effects become dominant. At a certain critical film thickness $t_c = R_p - R_k$, where R_p is the pore radius and R_k is the so-called core radius, pore condensation occurs, controlled by intermolecular forces in the core fluid. Hence, pore condensation occurs not in the entire pore but rather in the inner core.

Different models attempt to account for the multilayer (statistical) film thickness t_c by combining the Kelvin equation with a standard isotherm or a so-called t-curve, which usually refers to adsorption measurements on a nonporous solid. In the spirit of the Frenkel−Halsey−Hill theory the film thickness t on flat substrates is expected to vary with p as[54] $\ln(p/p_0) = -\alpha t^{-m}$, where α is the fluid−wall interaction parameter. In the case of nonretarded van der Waals fluid−wall interactions, m has the theoretical value 3. However, experimental values for m are often significantly smaller than the theoretical value, even for strongly attractive adsorbents such as graphite, i.e., $m = 2.5-2.7$.[54,55]

Pore condensation is often accompanied by hysteresis, i.e., capillary evaporation occurs at a lower relative pressure as capillary condensation. The details of sorption hysteresis depend on the thermodynamic state of the pore fluid and on the texture of the adsorbent, i.e., the presence of a pore network. It is now widely accepted that there is a correlation between the shape of the hysteresis loop and the pore size distribution, geometry and texture of the mesoporous adsorbent, although the detailed effects of these various factors on hysteresis are still not fully understood. An empirical classification of hysteresis loops is given by the IUPAC.[56] However, the mechanism and origin of sorption hysteresis is still a matter of discussion. There are essentially two models which contribute to the understanding of sorption hysteresis.[57,58]

(i) Independent (Single) Pore Model. Sorption hysteresis is considered as an intrinsic property of the phase transition in a single, idealized pore, reflecting the existence of metastable gas states.

(ii) Network Model. Sorption hysteresis is due to network effects, which reflect the shape of the pores, the distribution of pore sizes and their connectivity in the porous medium.

The network model takes into account that in real materials the pores are connected and form a three-dimensional network.[57,58,64−68] Specific network models were developed, where adsorption and pore condensation can be fully described in terms of thermodynamics. Capillary evaporation is essentially understood as caused by connectivity and pore blocking effects, which may lead to a percolation process. This would result in a steplike desorption branch, i.e., type H2 hysteresis (IUPAC classification) found for instance for the adsorption of fluids in porous Vycor glass.[58,59]

In contrast to the network model, theoretical approaches based on methods of statistical physics (e.g., density functional theory) support the picture that hysteresis may occur also in a single pore caused by the fact that the adsorption branch persists to the limit of metastability before jumping to the liquid branch.[58,60] In principle metastability is thermodynamically feasible on either branch, but in practice it occurs only during the adsorption process as the nucleation of the liquid capillary phase may be delayed. Assuming a pore of finite length, vaporization during the desorption process can occur via a receding meniscus; nucleation and therefore metastability do not occur during capillary evaporation.[63] Hence, the jump from liquid to gas on desorption occurs more likely at thermodynamic equilibrium. The independent (single) pore model to explain hysteresis is important for sorption isotherms exhibiting the hysteresis type H1, which was found to be characteristic for sorption isotherms of fluids in MCM-41 materials,[55] which consists of a one-dimensional channel system of cylindrical pores and in materials of well-defined pore shape and narrow pore size distribution like controlled-pore glasses[62,81] or ordered xerogels.[61]

In the case of sufficient wide mesopores the state of the pore fluid and the shift of the gas−liquid phase transition (pore condensation) from bulk coexistence can be expressed by classical approaches like the Kelvin equation in terms of macroscopic quantities. However, these macroscopic concepts do not account for the peculiarities of the critical region and cannot be applied to describe the state of the pore fluid in small mesopores anymore. Recently developed, microscopic theories based on recent advances in statistical mechanics as for instance the density functional theory (DFT),[70,71] lattice model calculation[72] and various computer simulation studies[69,73,74] provide a detailed description of the structure of fluids confined to narrow pores on a molecular level and have thus led to an improved understanding of the sorption and phase behavior of fluids in micro- and mesopores.

These microscopic models suggest, that a fluid in a pore can exist with two possible density profiles corresponding to inhomogeneous gas and liquid configurations in the pore. In this sense pore condensation is considered as a first order phase transition between an inhomogeneous gas configuration, which consists of vapor in the core region of the pore in equilibrium with a liquid like adsorbed film, and a liquid configuration, where the pore is completely filled with liquid. At the critical point of the confined fluid these two hitherto distinct fluid configurations, but with the same grand potential become indistinguishable.[71] However, the locus of the critical point of the pore fluid is not identical with the bulk critical point. The critical temperature of the confined fluid is shifted to lower temperatures, i.e., in contrast to the predictions of the Kelvin equation pore condensation and sorption hysteresis are not expected to persist up to the critical temperature T_c of the bulk fluid, but will vanish already at temperatures below T_c. The shift of the pore critical temperature is correlated with the pore width, i.e., the more narrow the pore, the larger is the shift of the pore critical temperature to lower temperatures.[71,75,76]

In addition to the shift in critical temperature, experiments and theory indicate that as a result of the combined effects of fluid-wall forces and finite-size the freezing temperature and triple point of the pore fluid may be also shifted to lower temperature relative to the bulk triple point,[77−79] if the wall fluid attraction is not too strong, i.e., the pore walls do not prefer the solid phase.[79] In fact, recent theoretical and experimental studies led to the conclusion that the complete coexistence curve of the confined fluid is shifted to lower temperature and higher mean density.[80−82] Hence, the shape of the observed sorption isotherms depends not only on the pore width, pore shape and texture of the porous material (as is reflected in the appropriate IUPAC classification of sorption isotherms and hysteresis loops), but also on the thermodynamic state of the confined fluid. Within this context one expects pore condensation and hysteresis to disappear already at temperatures, which are still below the bulk critical temperature, but may be observed even at temperatures below the bulk triple point. This has to be taken into account for the characterization of porous media by the analysis of appropriate sorption isotherms (e.g., nitrogen, argon and krypton sorption at 77 and 87 K). So far most systematic sorption studies on model adsorbents such as the M41S materials have concentrated on MCM-41.[83−92] The occurrence of sorption hysteresis of Type H1 (IUPAC Classification) in MCM-41 silicates and aluminosilicates, which consist of a one-dimensional channel system indicates that sorption hysteresis can be considered here in fact as an intrinsic property of the pore fluid and thus supporting the single pore model of sorption hysteresis.

To assess the influence of a well-defined three-dimensional pore network structure on pore condensation and hysteresis we performed systematic sorption studies on pure fluids in MCM-48 silicas. We present the first systematic study on the pore size- and temperature dependence of the sorption- and phase behavior of nitrogen, argon and krypton in the well defined, three-dimensional pore network of pristine mesoporous MCM-48 silica and MCM-48 silica/iron(III) oxide host−guest compounds. In addition, we compare the sorption and pore condensation behavior of argon in the small pores of MCM-48 silica (BJH pore diameter ca. 3 nm) and in the much wider pores of a controlled pore glass sample (mean pore diameter ca. 16 nm) at temperatures above and below the bulk triple-point temperature.

2. Experimental Section

2.1. Synthesis of Pristine Mesoporous MCM-48 Silica. The MCM-48 silicas were synthesized by stirring 1.0 moles of TEOS and 0.5 moles of KOH in 62 moles of H_2O for 10 min. After adding the cationic quaternary ammonium bromide surfactant (**A**: 0.7 moles of tetradecylammonium bromide (C_{14}TAB; Fluka); **B**, **D**: 0.65 moles of hexadecylammonium bromide (C_{16}TAB; Merck); **C**: 0.62 moles of octadecylammonium bromide (C_{18}TAB; Fluka)) and 10 min of vigorous stirring the white and creamy solution was filled into a Teflon-lined steel autoclave and statically heated at 388 K for 48 h. The resultant white precipitate was filtered and washed several times with warm deionized water. Drying gave a white powder which was calcined at 823 K in flowing air for 6 h giving the products **A**, **B**, **C**, and **D**.

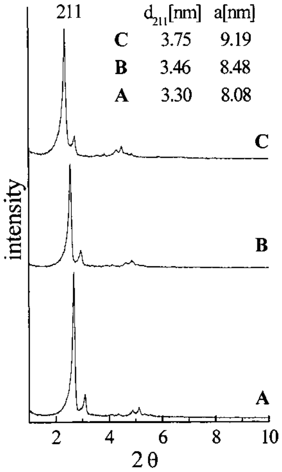

Figure 1. XRD patterns of three highly ordered pristine MCM-48 silica phases **A**, **B**, and **C**, which can be indexed in the space group $Ia\bar{3}d$.

2.2. Synthesis of MCM-48 Silica/Iron(III) Oxide Host−Guest Compounds. The impregnation procedure was carried out by stirring product **B** in a 1.6 M aqueous solution of iron(III) nitrate for 10 min. The dispersion was separated by centrifugation. The residue was dried in vacuum and calcined at 673 K in a N_2 flow for 6 h to yield the product **B−Fe$_2$O$_3$**.[42]

2.3. Sorption and Powder X-ray Diffraction Experiments. Nitrogen (purity 99.999 vol %), argon (purity 99.999 vol %) and krypton (purity 99.996 vol %) supplied by Messer Griesheim GmbH were used as adsorptives. In this work the sorption isotherms of nitrogen, argon, and krypton at 77 K (i.e., 77.35 K) and 87 K (i.e., 87.27 K) in different MCM-48 silica materials with BJH pore diameters 2−3 nm were determined in a pressure range from $p/p_0 = 0.005$ to 1 using a static volumetric technique (QUANTACHROME AUTOSORB). To investigate the existence of micropores in the material, argon sorption isotherms at 87 K in the range $p/p_0 = 1 \times 10^{-5}$ up to 1 were measured. The analysis station of the volumetric apparatus was equipped, in addition to the pressure transducers in the dosing volume of the apparatus, with high-precision pressure transducers (MKS Baratron) dedicated to read the pressure just in the sample cell from which adsorbed gas volumes are computed. Hence, the sample cell was isolated during equilibration, which ensured a very small effective void volume and therefore a highly accurate determination of the adsorbed amount. The saturation pressure p_0 was measured throughout the entire analysis by means of a dedicated saturation pressure transducer which allowed the vapor pressure to be monitored for each data point recorded. Before each sorption measurement the sample was outgassed at 393.15 K for 12 h under turbomolecular pump vacuum.

Powder X-ray diffraction patterns were recorded on a Bruker AXS D8 advance diffractometer (Cu Kα) in θ/θ geometry with a secondary monochromator.

3. Results and Discussion

3.1. Results of Systematic Sorption Studies on Nitrogen, Argon, and Krypton at 77 and 87 K in Different Pristine MCM-48 Silica Materials. *3.1.1. Characterization of Pristine MCM-48 Materials.* Figure 1 shows the XRD patterns of the three highly ordered pristine MCM-48 silica phases **A**, **B**, and

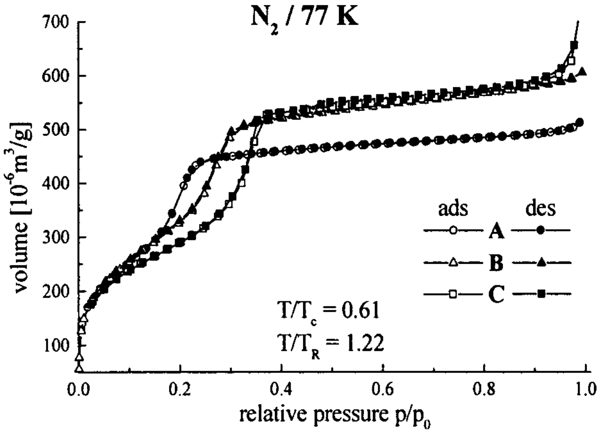

Figure 2. N_2 sorption isotherms (77 K) for pristine MCM-48 silica phases **A**, **B**, and **C**.

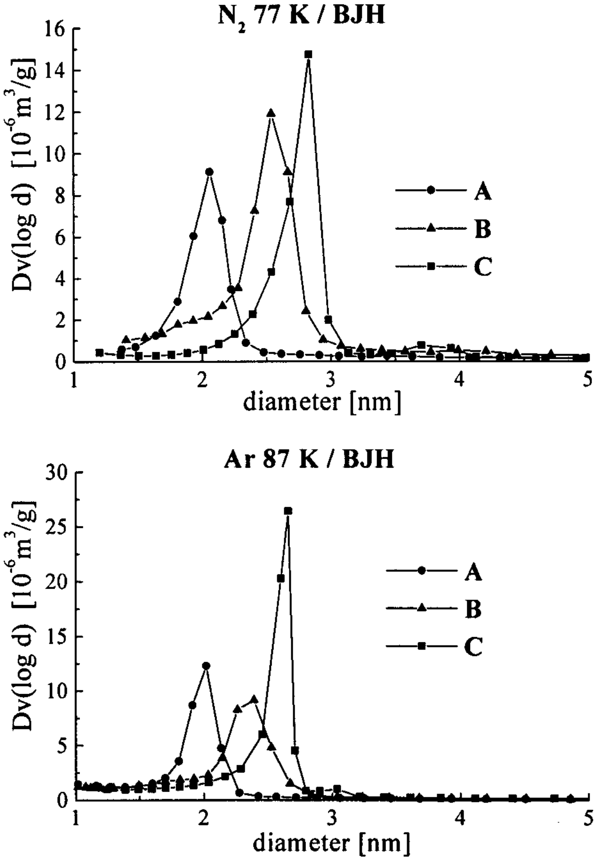

Figure 3. BJH pore size distributions ($Dv(\log d) \equiv dV/d(\log D)$) for pristine MCM-48 silica phases **A**, **B**, and **C** obtained from (a) N_2 sorption isotherms (77 K, Figure 2) and (b) Ar sorption isotherms (87 K, Figure 4).

C, which can be indexed in the space group $Ia\bar{3}d$. As a function of the increasing carbon chain length within the series of **A**, **B**, and **C**, the reflections are shifted to lower 2θ values and higher d spacing, respectively.

In Figures 2 and 4 nitrogen and argon sorption isotherms measured at 77 and 87 K for different pristine MCM-48 materials are shown. The N_2 isotherms at 77 K as well as the sorption isotherms of Ar at 87 K reveal for MCM-48 phases **A** and **B** reversible pores condensation at relative pressures $p/p_0 < 0.4$ with no sorption hysteresis. With increasing pores size the occurrence of pore condensation is shifted to higher relative pressures as expected from classical theories of pore condensation.

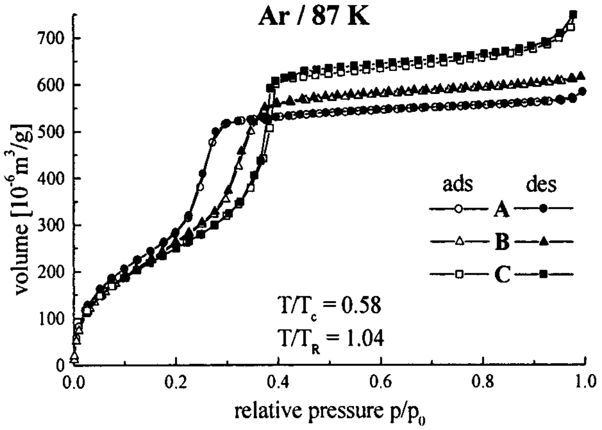

Figure 4. Argon sorption isotherms (87 K) for pristine MCM-48 silica phases **A**, **B**, and **C**.

Pore condensation accompanied by hysteresis could be observed for argon sorption at 87 K in sample **C** in a relative pressure range p/p_0 0.365−0.413. (In addition in the same isotherm a very small hysteresis loop at relative pressures > 0.4 could be detected, which may be caused by larger meso- and macropores combined with pore blocking, i.e., networking effects). The MCM-48 silica phases exhibit no microporosity as revealed by measurements in the low-pressure region and by appropriate *t*-plots.

Different methods were used to analyze the nitrogen isotherms on the pristine MCM-48 materials with respect to surface and pore size characteristics. In Table 1 appropriate results for the pristine MCM-48 materials and the MCM-48 silica/iron(III) oxide host compound **B−Fe₂O₃** are summarized. In the following section we discuss only results for the pristine MCM-48 materials; the pore size characteristics of B−Fe_2O_3 will be discussed in section 3.2.2. The results given in Table 1 indicate that specific surface areas decrease, but the pore widths and pore volumes increase from MCM-48 silicas **A**−**C**. The BET surface areas were determined from nitrogen isotherms at 77 K in a range of relative pressures p/p_0 prior to the occurrence of pore condensation for each sample (**A**, 0.07−0.15; **B**, 0.07−0.15; **C**, 0.07−0.25) by taking the cross-sectional area of a nitrogen molecule as 0.162 nm^2. However, as already indicated for small pore MCM-41 material,[86] the BET method is inaccurate for estimating the surface area for MCM-48 materials because pore condensation also occurs within the relative pressure range 0.05−0.3, where the BET theory is usually considered to be valid. Thus, pore filling is observed at pressures very close to the pressure range where monolayer−multilayer formation on the pore walls occurs.

Most classical methods used for the analysis of mesopore size distributions (PSD) from sorption isotherms, like the most prominent method of Barett, Joyner, and Halenda (BJH)),[54,93] are based on macroscopic thermodynamic models such as the modified Kelvin equation (see eq 1). We applied the BJH method to derive from nitrogen (77 K) and argon (87 K) isotherms the pore size distributions of the MCM-48 phases. In both cases the BJH pore size distributions were calculated from the desorption branches of the sorption isotherms by estimating the (statistical) thickness t_c of the adsorbed film at the pore walls $t_c = R_p - R_k$, where R_p is the pore radius and R_k is the Kelvin or core radius by employing the Frenkel-Halsey-Hill approach. The BJH pore diameter (maximum of pore size distribution curves) calculated from nitrogen and argon adsorption isotherms are in good agreement with each other as shown in Figure 3. The obtained narrow pore size distributions and

TABLE 1: Characterization of the Pristine MCM-48 Silica Phases and MCM-48 Silica Iron(III) Oxide Host/Guest Compound B−Fe_2O_3 with Respect to Specific Surface Area, Pore Size, and Pore Volume Using Various Methods[a]

adsorbent	S_{BET,N_2}, [m^2/g]	V_{p,N_2}, [10^{-6} m^3/g]	d_{p,N_2}(BJH), [nm]	D_{h,N_2}, [nm]	$d_{p,Ar}$(BJH), [nm]	$d_{p,Ar}$(SF), [nm]	$V_{p,Ar}$(SF), [10^{-6} m^3/g]
A	1261	0.70 ($p/p_0 = 0.32$) 0.77 ($p/p_0 = 0.95$)	2.05	2.21	2.02	2.42	0.68
B	1202	0.81 ($p/p_0 = 0.40$) 0.91 ($p/p_0 = 0.95$)	2.52	2.68	2.39	2.86	0.72
C	1078	0.82 ($p/p_0 = 0.40$) 0.95 ($p/p_0 = 0.95$)	2.81	3.04	2.65	3.31	0.78
B−Fe_2O_3	695	0.40 ($p/p_0 = 0.40$) 0.45 ($p/p_0 = 0.95$)	2.23	2.31	2.16	2.61	0.38

[a] S_{BET}: BET-specific surface area. d_p(BJH): BJH-mode pore diameter. $D_h = 4V_p/S_{BET}$: average pore diameter. In addition, argon sorption isotherms at 87 K for both materials were analyzed with respect to pore size (d_p(SF)) and pore volume (V_p(SF)) by applying the Saito−Foley method.

the powder X-ray diffraction patterns (see Figure 1) indicate both that the MCM-48 materials investigated in this work are highly ordered.

Pore volumes were calculated from the measured adsorbed gas volume by assuming the density of the capillary fluid to be equal to the density of liquid bulk nitrogen at the same temperature (Gurvich method[54]). Using the values of the pore volumes determined in this way (at $p/p_0 \approx 0.4$) allows the determination of the average pore diameter for the primary mesopore system of MCM-48 according to $D_h = 4V_p/2S_{BET}$. As indicated in Table 1 the obtained values for D_h are slightly higher than the BJH pore diameters. The average pore diameter D_h is defined for a mesopore structure, which consists of a set of open-ended nonintersecting cylinders and is based on the assumption that the specific surface area is confined to the cylindrical pore walls. This condition should be fulfilled in the case of the one-dimensional channel system of the MCM-41 phase. However, although MCM-48 comprises of two three-dimensional pore systems, the D_h pore diameters are still in reasonable good agreement with the BJH values.

In addition, the Saito−Foley (SF) method,[94,95] which is an extension of the original Horvath−Kawazoe (HK) method[96] for slit-pore geometry (i.e., nitrogen/carbon system), was applied to the argon data at 87 K. The Saito−Foley method is based on a fundamental statistical analysis of a fluid (argon) confined to a microporous cylindrical-pore (zeolite) including details of the fluid−wall interaction. The HK and SF methods are widely used, and provide, because they take into account details of the solid−fluid attractive forces in narrow pores, a better measure for micropore filling pressures than the macroscopic, classical methods of micropore analysis. It is assumed that the filling of micropores takes place at a characteristic relative pressure, which is directly related to the fluid−solid interaction energy and the effective pore radius. Thus, micropores can either be full or empty according to whether the pressure of the adsorptive is higher or less than the value characteristic for a particular diameter, which is similar to the pore filling mechanism of pore condensation in the mesopore range. Hence, some workers applied the SF method also for pore size determination in narrow cylindrical mesopores of MCM-41 materials[92,97] and good agreement between pore diameters determined by the SF method and Kelvin equation based methods were reported.[97] This is remarkable because as described above the SF method is originally dedicated to microporous materials.

Within this context we applied the SF method also to our argon sorption isotherms of MCM-48 silica. As shown in Table 1 the SF values obtained for pore volumes are in good agreement with the (Gurvich) pore volumes obtained from the nitrogen isotherms at ca. $p/p_0 = 0.4$, which corresponds to the plateau of the sorption isotherm after pore condensation has occurred in the primary mesopores of MCM-48. In addition the SF pore diameters are still in the same range as the BJH and average pore diameters.

However, it should be noted, that classical methods such as BJH, which are based on macroscopic, thermodynamic assumptions provide not a reliable basis for the calculation of pore widths H below 7−8 nm in the case of porous carbon materials,[69] and for pore diameters < ca. 3.5 nm in the case of oxide materials.[74] These classical approaches are macroscopic in a sense that they do not start from a well-defined molecular model, so that a connection between molecular behavior and macroscopic properties (like the surface tension or densities of coexisting phases) is not defined. In narrow pores attractive fluid−wall interactions become dominant, so that the concept of a smooth liquid−vapor interface and bulk-like core fluid cannot realistically be applied. In contrast, DFT and molecular simulation (Monte Carlo and Molecular Dynamics) provide more accurate methods on the basis of an accurate molecular theory. Hence, pore sizes obtained by application of the BJH method should be regarded as apparent rather than real pore sizes, although a number of studies revealed that pore sizes calculated with the BJH approach are still probably in the right range.[55] Compared with new methods that rely on microscopic descriptions such as the density functional theory (DFT) and Monte Carlo computer simulation (MC), the macroscopic thermodynamic methods underestimate the calculated pore diameter by ca. 1 nm.[74,90,98] However, it should be noted that a new method, combining the Kelvin equation with an improved model of the statistical adsorbed film thickness, has very recently been proposed.[99] The pore filling pressures obtained with this method are in good agreement with DFT results, except for narrow micropores.

3.1.2. Pore Condensation and Hysteresis Behavior of Nitrogen, Argon, and Krypton in Pristine MCM-48 Silica Materials. As already described in section 3.1.1, nitrogen isotherms at 77 K ($T/T_c = 0.61$, where $T_c = 126.20$ *K* is the critical temperature of the bulk fluid; $T/T_r = 1.22$, where $T_r = 63.15$ *K* is the triple-point temperature of the bulk fluid) show for all sorption isotherms pore condensation without hysteresis (Figure 2). The argon isotherms at 87 K ($T/T_c = 0.58$, $T_c = 150.66$ K; $T/T_r = 1.04$; Figure 4) reveal also reversible pore condensation for **A** and **B**, but in the case of **C** a small hysteresis loop can be detected. With increasing pore size the occurrence of pore condensation is shifted to higher relative pressures as expected from classical theories of pore condensation. In contrast to the nitrogen isotherms at 77 K and argon sorption isotherms at 87 K the argon isotherms at 77 K ($T/T_c = 0.51$; $T/T_r = 0.92$; $T_R - T = 6.8$ K, where $T_R = 83.81$ *K* is the triple-point temperature of the bulk fluid) reveal for all MCM-48 silicas studied here pore condensation accompanied by hysteresis (Figure 5). A

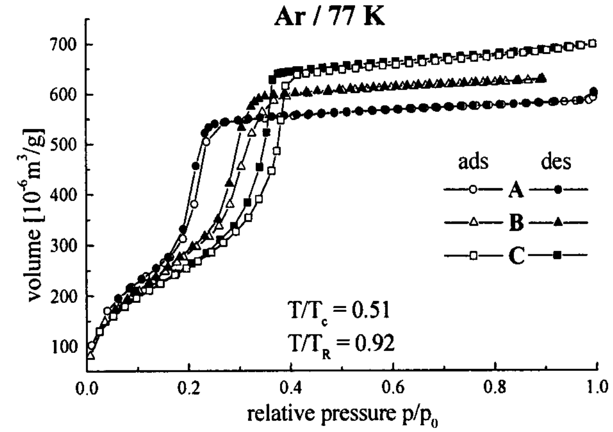

Figure 5. Argon sorption isotherms (77 K) for pristine MCM-48 silica phases **A**, **B**, and **C**.

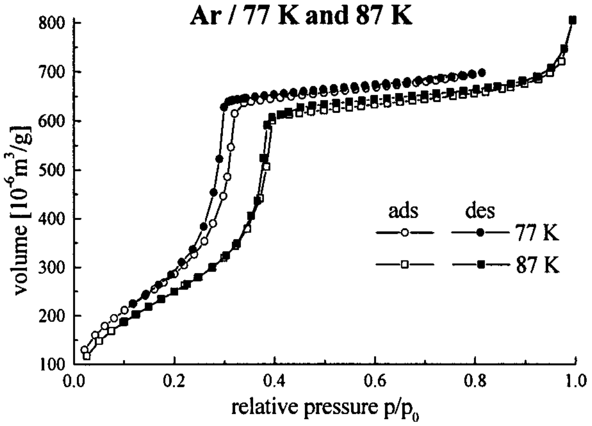

Figure 6. Comparison of argon sorption isotherms (87 and 77 K) for MCM-48 silica phase **C**. Here, the saturation pressure of undercooled liquid argon is chosen as p_0 for the correspondent sorption isotherm at 77 K.

qualitatively similar pore condensation and hysteresis behavior of argon sorption at 77 and 87 K was recently also observed for MCM-41 silica phases.[92] As shown in Figure 5, the widths of the hysteresis loops of the sorption isotherms decrease with decreasing pore width, indicating that the fluid confined to the pores in phase **A** may be closer to pore criticality as the fluid confined in the pores of **C** at 77 K ($T_c - T = 73.3$ K). According to theoretical predictions[58,71] it is expected that, at constant temperature, pore criticality can be approached by reducing the pore diameter.

In all cases the steep portions (pore condensation steps) of the argon isotherms are much sharper than the corresponding nitrogen isotherms and the adsorbed amount after the pores are filled is higher because of the smaller size of the argon molecule and the higher density of liquid argon ($\rho^l = 1.396$ g cm^{-3} at 87.29 K) compared to liquid nitrogen ($\rho^l = 0.870$ g cm^{-3} at 77.35 K). However, we note that also the argon pore condensation steps are smeared out over a finite pressure range for two reasons: (i) the nonvanishing width of the pore size distribution of the present material (cf. Figure 4); (ii) intrinsic feature of phase transitions in systems of small size,[71] i.e., in small cylindrical pores a rounding of the first-order phase transition caused by finite size effects is to be expected.

The reversible pore condensation at $p/p_0 < 0.4$ observed for nitrogen sorption at 77 K in the MCM-48 silicas used in this study was also observed in MCM-41 silica materials of pore diameters 2−4 nm.[83−92] These observations are in accordance with the expectation that the lower closure point for nitrogen sorption hysteresis at 77 K is around $p/p_0 = 0.42$, which was originally considered as the limit of thermodynamic stability of the liquid nitrogen meniscus. Recent theoretical studies[100] and computer simulations[101] indicate that pore wall roughness and details of the fluid-wall interaction may also be significant for the disappearance of nitrogen sorption hysteresis in M41S materials.

In a comprehensive discussion on the lack of hysteresis in N_2 isotherms at 77 K in MCM-41,[89] it was assumed that the absence of experimental hysteresis of samples with mean pore size ca. 4 nm cannot be explained by the capillary critical temperature for a given pore size being achieved. Pore condensation without hysteresis was also observed for SF_6 confined to controlled pore glass[81] and in novel ceramic silica materials of mean pore sizes < 3.5 nm[102] in a temperature range from the triple point up to the pore critical temperature. Accordingly, one would expect that sorption hysteresis disappears already in a certain temperature range below the pore critical temperature. The observed disappearance of sorption hysteresis in the temperature range from 77 to 87 K for argon sorption in the MCM-48 silicas **A** and **B** is consistent with this picture as well as the decrease of the width of hysteresis loop for MCM-silica **C** as shown in Figure 6. For the comparison of the temperature dependence of the hysteresis and pore condensation behavior of sample **C** the saturation pressure of the undercooled liquid ($p_{0,\mathrm{liquid}} = 229.1$ Torr)[105] was chosen as p_0 in the case of the 77 K sorption isotherm, also because it can be assumed that the capillary phase at this temperature is still liquid.[91,90] However, in general the choice of the supercooled liquid p_0 as a reference state is not straightforward because $T < T_R$. As also discussed in context with the results shown in Figure 7, there are arguments to choose the saturation pressure of the solid instead.[54,55] The disappearance of hysteresis for argon sorption isotherms at 87 K in the pore diameter (d_p,N_2(BJH)) range from 2.81 nm (sample **C**) to 2.52 nm (sample **B**) is again in agreement with the expectation that for a given temperature pore criticality is approached with decreasing pore diameter.[71] The difference in the occurrence of hysteresis for nitrogen and argon at 77 K can be explained as a consequence of the lower reduced temperature of argon ($T/T_c = 0.51$) compared to nitrogen ($T/T_c = 0.61$).

To compare the sorption behavior of fluids in the small mesopores of MCM-48 silica with the pore condensation and hysteresis behavior in much larger silica pores, we have also studied the argon sorption behavior at 87 and 77 K in controlled-pore glass (supplied by BAM, Germany; $d_{p,N2}$(BJH) = 16 nm, $S_{BET} = 120$ m^2/g, $V_p = 0.63 \times 10^{-6}$ m^3/g), which consists of an interconnected pore system with narrow pore size distribution. In Figure 7 the pore condensation and hysteresis behavior of argon at 87 and 77 K in a well-defined MCM-48 phase (sample **D**, $d_{p,N2}$(BJH) = 2.67 nm, $S_{BET} = 1060$ m^2/g, $V_p = 0.88 \times 10^{-6}$ m^3/g) is compared with the behavior in the controlled-pore glass. Figure 7a (Ar, 87 K) shows pore condensation and hysteresis for the argon sorption isotherm in CPG, and reversible pore condensation for argon in MCM-48. The adsorbed amount of fluid in MCM-48 is much higher in comparison to controlled pore glass, which is due to the much higher specific surface area and pore volume of MCM-48. This sorption behavior underlines the unique texture of MCM-48 and its potential for several practical applications in comparison with other well-defined mesoporous materials.

In contrast to the argon sorption behavior at 87 K, Figure 7b shows that at 77 K pore condensation and hysteresis occurs only

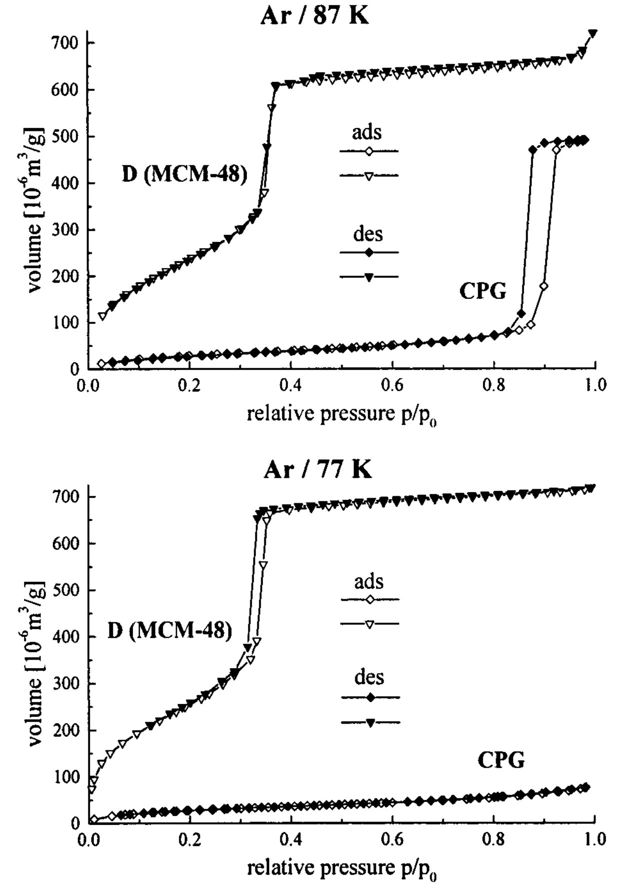

Figure 7. Temperature dependence of sorption hysteresis for argon sorption in MCM-48 silica material **D** [$d_{p,N2}$(BJH) = 2.67 nm] and for comparison in controlled-pore glass [$d_{p,N2}$(BJH) = 15.7 nm]. (a) 87 K, (b) 77 K, p_0 represents the saturation pressure of solid argon at 77.

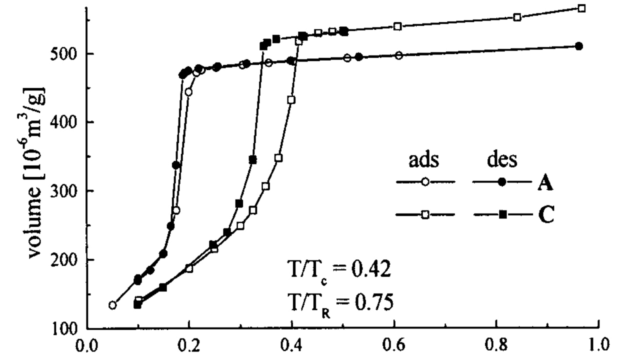

Figure 8. Krypton sorption (87 K) for pristine MCM-48 silica materials **A** and **C**. The chosen p_0 value is the saturation pressure of solid krypton at 87 K.

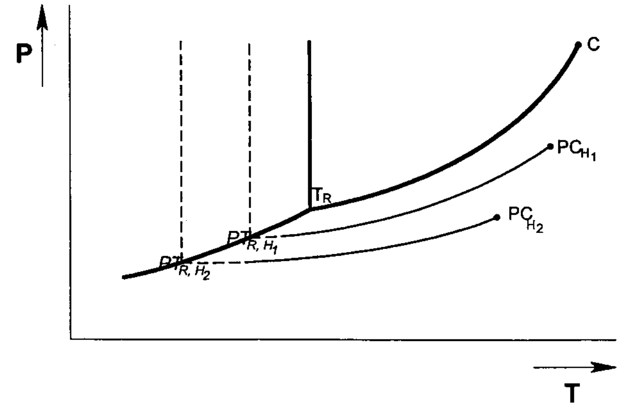

Figure 9. Schematic *p*−*T* diagram of a bulk fluid and pore fluid confined to different-sized pores (width $H_1 > H_2$, see text).

in MCM-48, but not in CPG. The observed very different sorption and pore condensation behavior for the systems argon/MCM-48 and argon/CPG at 87 and 77 K reflects that for a given temperature the thermodynamic state of the confined fluid is different in the narrow pores of MCM-48 compared to the much larger pores of CPG.

Phase transitions of the pore fluid were also observed for krypton in MCM-48 silica materials at 87 K ($T/T_c = 0.42$, $T_c = 209.4$ K) which is 28.5 K below the bulk triple-point temperature ($T_R = 115.8$ K). The sorption isotherm at 87 K for **A** and **C** presented in Figure 8, exhibit both a hysteresis loop of type H1, which is much broader in width for **C** as compared to **A**, i.e., as in the case of the argon isotherms at 77 K the width of the hysteresis loop decreases with decreasing pore width, indicating that at a certain pore width the occurrence of a first-order phase transition is not possible anymore. To explain the observed pore size dependence of the sorption hysteresis one could argue similar as in the case of the argon isotherms at 77 K, that the pore fluid of **A** ($d_{p,N2}$(BJH) = 2.05 nm) is much closer to pore criticality as the confined fluid in **C** ($d_{p,N2}$(BJH) = 2.81 nm). However, the nature of the observed phase transitions ca. 122 K below the bulk critical temperature and 28.5 K below the bulk triple point is not clear. In fact, in a recent paper the observation of a solidification of the krypton capillary phase at 77 K[95] in the pores of MCM-41 (mean pore diameter ca. 4 nm) was reported by employing microcalorimetric techniques, neutron diffraction and sorption measurements. In addition, a systematic study of adsorption hysteresis of different gases (CO_2, Xe, N_2) in porous Vycor glass (mean pore diameter ca. 6 nm) in a temperature range from well below the bulk triple-point temperature up to the critical temperature revealed the disappearance of sorption hysteresis on approaching the bulk critical temperature and in a temperature range below the bulk triple point, indicating a critical point shift to lower temperature and a closure of the (hysteresis) phase diagram of the pore fluid below the triple-point temperature of the bulk fluid.[106] Also with respect to these observations the sorption behavior of krypton in the MCM-48 silicas will be investigated in more detail in a further study.[103]

To discuss the described different sorption and phase behavior of krypton and argon in MCM-48 silica and controlled-pore glass at temperatures below the bulk triple-point temperature in more detail, we employ a schematic (*p*−*T*) diagram (Figure 9) of a fluid confined to pores of different widths H_1 and H_2 ($H_1 > H_2$) together with the *p*−*T* diagram of the bulk fluid (bold lines). This schematic phase diagram is based on results obtained in theory, computer simulations and experiments in recent years.[71,77−82] The pore condensation line of a pore fluid, which defines the locus of states of the unsaturated vapor at which pore condensation will occur in pores of given size and shape, terminates in a pore critical point (PC_{H1} and PC_{H2}), which is shifted to lower temperature and pressure with respect to the bulk fluid. Moreover, the pore condensation lines are expected to extend down to an appropriate pore triple point ($PT_{R,H2}$ and $PT_{R,H1}$), which may also be shifted to lower temperature. In such a case the shift of the pore triple-point temperature compared to the bulk value is expected to increase with decreasing pore width.[77−79] Unfortunately, compared with the relatively large number of publications in recent years dealing with pore criticality, not much work is published so far concerning the details of the phase diagram of a pore fluid below the bulk triple point. As a consequence the locus ($p-T$) of the pore triple point in a general phase diagram is not very well-known. Because of this situation the pore condensation and freezing lines for the pore fluid in the low-temperature region are shown as dashed lines indicating the speculative status of the low-temperature region in the schematic phase diagram.

However, a similar phase diagram as shown in Figure 9 was indeed derived for CO_2 confined to porous Vycor glass from positron and positronium annihilation experiments.[78] In these experiments it was found that the pore condensation line terminates in a (*quasi*) pore triple point, which is reduced both in temperature and pressure from that of the bulk. Similar results were obtained from a Monte Carlo simulation of a Lennard Jones fluid confined to a slit pore.[79] Under consideration of these results the very different argon sorption behavior observed for MCM-48 silicas and controlled-pore glass at 87 and 77 K described above may be discussed in the following way: At 87 K (Figure 7a) pore condensation occurs for argon in CPG and MCM-48 silica, which indicates that in both cases the pore condensation line (see Figure 9) is crossed below the pore critical temperature. Hysteresis is observed for the Ar/CPG system but not in the narrow pores of MCM-48 silica, in accordance with theoretical expectations,[71] that at a given temperature hysteresis should eventually disappear with decreasing pore size. The lack of pore condensation and hysteresis for argon at 77 K (Figure 7b) in CPG indicates however that there is no extension of the pore condensation line down to this temperature (which is ca. 6.5 K below the triple-point temperature of the bulk fluid) at pressures lower than the corresponding sublimation pressure of the bulk fluid. Only adsorption exists in the pores without any phase transition until solidification of the bulk fluid occurs (in the case of Ar sorption at 77 K the saturation pressure of Ar solidified in a special p_0-cell was measured simultaneously during the sorption experiment; $p_{0,\mathrm{solid}} \approx 195$ Torr). However, the sorption isotherms of Ar in MCM-48 still reveal pore condensation and sorption hysteresis at 77 K, indicating that here in contrast to the Ar/CPG system the pore condensation line extends at least down to this temperature. This implies that the (quasi) triple point of the confined argon in MCM-48 silica of pore diameter (d_p,N_2(BJH) $\leq$ ca. 3 nm) is shifted more than ca. 6.5 K to lower temperature compared to bulk argon.

It is often argued[54,55] that the saturation pressure of supercooled liquid argon should be employed instead of the saturation pressure of solid argon at 77 K (as used in this study). In this case one may conclude that it is not possible to measure a complete argon isotherm at 77 K as bulk solidification occurs before the saturation pressure for liquid argon is achieved, which would lead to a truncated isotherm without capillary condensation and hysteresis for argon in CPG at this temperature. However, this would mean that for 77 K ($T_R - T \approx 6.5$ K) the pore condensation pressure would be higher than the corresponding sublimation pressure of the bulk fluid, indicating that for the system Ar/CPG the pore condensation line would cross the bulk sublimation line somewhere below the bulk triple-point temperature but above 77 K. However this is not to be expected from a theoretical point of view: For instance, in a recent free-energy study Dominguez et al.[79] calculated the complete phase diagram for weakly attractive and repulsive walls; their results did not show any indication for such a crossing of the bulk sublimation line by the pore condensation line. Hence, one may conclude that pore condensation of argon in the pores of CPG does not occur at 77 K, because this temperature seems to be already below the (quasi) pore triple-point temperature of the confined argon. Further work is necessary to come to a more comprehensive understanding of the observed phenomena.[103]

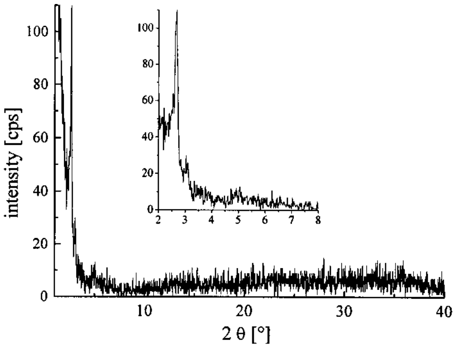

Figure 10. XRD pattern of the mesoporous host−guest compound **B−Fe$_2$O$_3$**. The inset shows an enlargement of the low-angle region.

3.2. Results of Systematic Sorption Studies on Nitrogen, Argon, and Krypton at 77 and 87 K in MCM-48 Silica/Iron(III) Oxide Host Compound. *3.2.1. Characterization of MCM-48 Silica/Iron(III) Oxide Host−Guest Compound.* Because of their specific pore structure the cubic MCM-48 phase is considered as a matrix to accommodate certain guest compounds. We have focused our work especially on the cubic MCM-48 phase because the channels within the three-dimensional pore structure of MCM-48 contain intersections which allow a higher accessibility to catalytic sites. As already described in the Experimental Section, the introduction of iron oxide into mesoporous MCM-48 phase **B** was performed by wet impregnation technique. A decoration/coating of the inner surface of the silica walls was indicated by HRTEM, EDX investigations and the existence of small, slightly disordered iron(III) oxide nanoparticles was proved by X-ray absorption spectroscopic measurements.[42] The respective XRD pattern of sample **B−Fe$_2$O$_3$** is shown in Figure 10. The 211 and 220 reflections of the mesoporous silica host-structure are clearly observable. Nevertheless, the overall intensities are reduced in comparison to the pristine material. This a common effect because the introduction of scattering material into the pores leads to an increased phase cancellation between scattering from the wall and the pore regions and therefore to reduced scattering intensities of the Bragg reflections.[42] The possible formation of a crystalline bulk phase of iron(III) oxide can be excluded because no XRD pattern of the corresponding can be detected.

An additional indication for a decoration/coating of the inner surfaces by iron(III) oxide should be the observation of a decrease of the pore diameter. Whereas the sorption properties of the pristine MCM-48 phase **B** were already described extensively in section 3.1, we report here nitrogen, argon, and krypton sorption data obtained for the impregnated phase. Different methods were used to analyze nitrogen (77 K) and argon sorption (87 K) isotherms to obtain surface and pore size characteristics for **B** and **B−Fe$_2$O$_3$**. The correspondent results are shown in Table 1. The in-situ formation of iron(III) oxide within the pores of the pristine MCM-48 silica phase results in a decrease of specific surface area, pore volume, and pore diameter. A direct comparison of BJH pore size distribution curves obtained from nitrogen isotherms (77 K) and argon sorption isotherms (87 K) for **B** and **B−Fe$_2$O$_3$** is shown in Figure 11a,b (the appropriate sorption isotherms are shown in Figures 2, 4 and 12, 13b, respectively). Argon and nitrogen BJH curves reveal both a decrease in the BJH mode diameter of phase **B−Fe$_2$O$_3$**, whereas the width of the pore size distribution is similar in both cases. Although the absolute values obtained

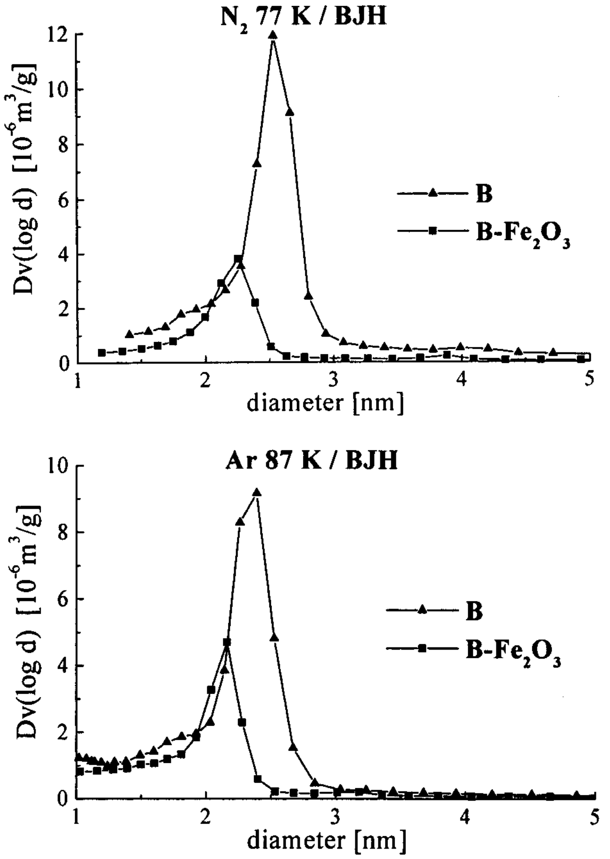

Figure 11. Pore size distributions ($Dv(\log d) \equiv dV/d(\log D)$) for (a) MCM-48 silica/iron(III) oxide host−guest compound **B−Fe$_2$O$_3$** and pristine MCM-48 phase **B** obtained from N$_2$ sorption isotherms (77 K, Figures 12 and 2) and (b) MCM-48 silica/iron(III) oxide host−guest compound **B−Fe$_2$O$_3$** and pristine MCM-48 phase **B** obtained from argon sorption isotherms (87 K, Figures 13b and 4).

for the BJH and SF (Ar, 87 K) pore diameters are slightly different, in all cases the pore diameter of the impregnated MCM-48 silica phase was lowered of about 0.2−0.3 nm compared to the pristine MCM-48 phase. A similar shift of the pore diameter was obtained by calculating the average pore diameter according to $D_h = 4V_p/S_{BET}$, by assuming cylindrical pores. In conclusion, these results still reveal mesoporosity for the MCM-48 silica/iron(III) oxide system, accompanied by a reduction of the pore width, which is together with results from HRTEM, EDX, and XAFS[42] a good indication for a coating of the inner surface of the silica walls.

3.2.2. Pore Condensation and Hysteresis Behavior of Nitrogen, Argon, and Krypton in MCM-48 Silica/Iron(III) Oxide Host−Guest Compound. Sorption isotherms of nitrogen, argon and krypton for MCM-48 silica/iron(III) oxide host−guest compound **B−Fe$_2$O$_3$** are shown in Figures 12−14. The nitrogen sorption isotherms at 77 and 87 K on **B−Fe$_2$O$_3$** depicted in Figures 12 and 13 reveal a small step due to pore condensation, but no hysteresis. The temperature dependence of the pore filling step of nitrogen isotherms is shown in Figure 13a. At higher temperature (87 K) the relative pressure for pore filling is shifted to higher value and the adsorbed amount is smaller as compared to 77 K. This behavior is expected from classical theories of pore condensation and from the fact that the density of the capillary liquid decreases slightly with increasing temperature.

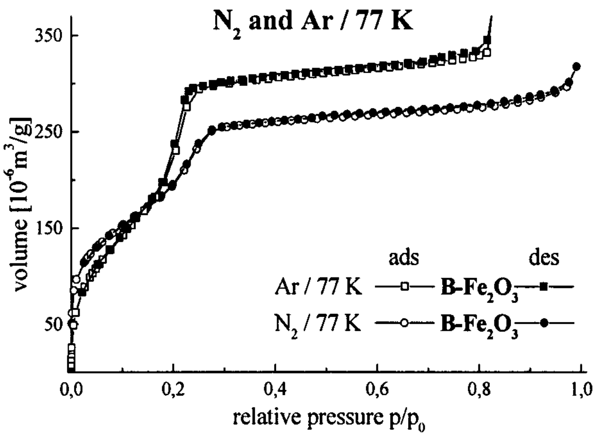

Figure 12. Comparison of nitrogen and argon sorption behavior (77 K) in MCM-48 silica/iron(III) oxide host−guest compound **B−Fe$_2$O$_3$**. In the case of the Ar isotherm p_0 represents the saturation pressure of the undercooled liquid argon.

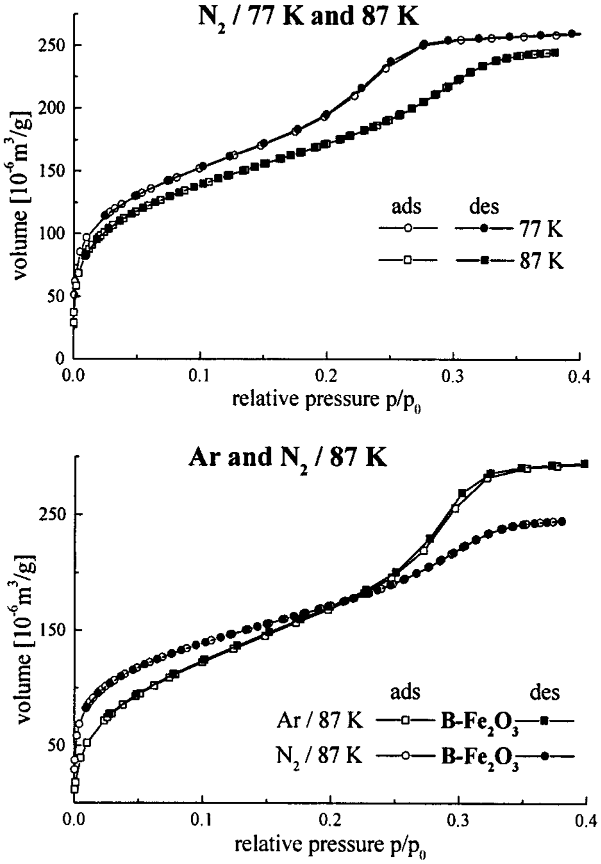

Figure 13. (a) Nitrogen sorption in MCM-48 silica/iron(III) oxide host−guest compound B−Fe$_2$O$_3$ at 77 and 87 K (Enlargement of the sorption isotherm up to relative pressure of ca. 0.4). (b) Comparison of nitrogen and argon sorption behavior (87 K) in MCM-48 silica/iron(III) oxide host−guest compound B−Fe$_2$O$_3$ (Enlargement of the sorption isotherm up to relative pressure region of ca. 0.4.)

A comparison between the sorption and pore condensation behavior of argon and nitrogen in **B−Fe$_2$O$_3$** at 77 K is made in Figure 12. For the argon isotherm at 77 K the saturation pressure of the undercooled liquid was taken as reference (instead of the solid) in order to compare with the nitrogen isotherm at 77 K. Figure 12 shows that the adsorbed amount for nitrogen is higher at lower pressures, but then the sorption isotherms cross at a relative pressure p/p_0 ca. 0.15 due to the onset of pore condensation for the **Ar/B−Fe$_2$O$_3$** system. The pore-filling step for **N$_2$/B−Fe$_2$O$_3$** occurs at a slightly higher relative pressure. The argon isotherm reveals a much more pronounced pore condensation step and the adsorbed amount corresponding to the plateau of the sorption isotherm is higher as for the nitrogen

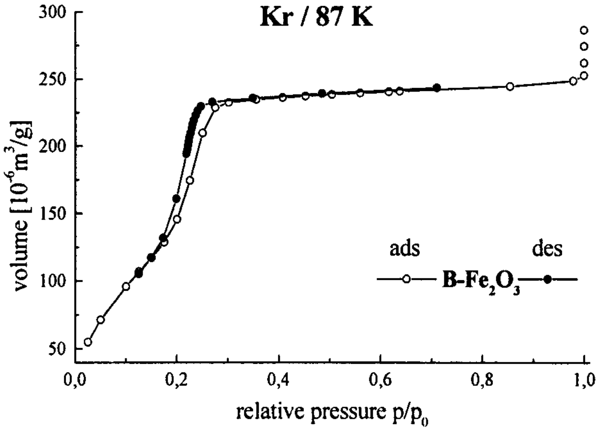

Figure 14. Krypton sorption (87 K) in MCM-48 silica/iron(III) oxide host−guest compound **B−Fe$_2$O$_3$**. The chosen p_0 value is the saturation pressure of solid krypton at 87 K.

isotherm, due to the smaller molecule size and the higher liquid density of argon compared to nitrogen. For the argon sorption isotherm at 77 K even a small hysteresis loop could be resolved, which disappears at 87 K, as shown in Figure 13b, where argon and nitrogen sorption behavior at 87 K is shown up to a relative pressure of ca. 0.4. Similar to the isotherms at 77 K the argon isotherms reveal a much sharper pore filling step; a crossing of the nitrogen and argon sorption isotherms occurs at a relative pressure of p/p_0 = ca. 0.22.

While for argon and nitrogen sorption isotherms at 87 K no sorption hysteresis could be observed anymore, the appropriate krypton sorption isotherm on **B−Fe$_2$O$_3$** (Figure 14) reveals a clear hysteresis loop in agreement with the krypton isotherms measured at the same temperature for pristine MCM-48 silica materials. The steep increase of the krypton sorption isotherm at p/p_0 ca. 1 (p_0 is the saturation pressure of solid krypton) indicates the solidification of bulk krypton.

The different behavior of nitrogen, argon, and krypton at 87 K reflect as discussed in section 3.1.2 different thermodynamic states of the pore fluid compared to the bulk fluid. The nature of the phase transition observed for krypton at 87 K, i.e., ($T_c - T \approx 122$ K; $T_R - T \approx 28.5$ K) will be explored as already mentioned in a forthcoming paper.[103]

Summarizing, it can be stated that the sorption and phase behavior of nitrogen, argon and krypton in MCM-48 silica/iron(III) oxide host compound is qualitatively similar to the behavior observed in pristine MCM-48 silica materials. The results indicate that the mesoporous host-structure is still intact in **B−Fe$_2$O$_3$**.

4. Summary and Conclusions

A systematic study on the sorption- and phase behavior of nitrogen, argon and krypton at 77 and 87 K was performed for different, highly ordered pristine mesoporous MCM-48 silica materials and for a MCM-48 silica/iron(III) oxide host−guest compound with pore diameter < 4 nm. Different methods (BJH, SF, Gurvich) were applied for pore size analysis of pristine MCM-48 silicas; the obtained values for the pore volumes and diameters were in reasonable good agreement with each other.

Pore condensation was found to be more pronounced for argon sorption isotherms obtained at 87 K compared with nitrogen sorption isotherms at 77 K on the same MCM-48 material. Hence, the argon sorption data at 87 K may be better suited for pore size analysis of M41S materials, which consist of relatively small mesopores. The analysis of nitrogen and argon sorption isotherms at 77 and 87 K indicates that the impregnation of a pristine MCM-48 silica phase with iron(III) oxide has led indeed to a coating of the inner pore walls. In addition, the observed sorption and pore condensation behavior of nitrogen, argon and krypton in MCM-48 silica/iron(III) oxide was found to be qualitatively similar as for pristine MCM-48 silica materials, which indicates that the mesoporous host structure is still intact.

The current work shows that also for MCM-48 silica phases the occurrence of sorption hysteresis depends on temperature and pore size, i.e., the thermodynamic states of pore fluid and bulk fluid. Nitrogen sorption isotherms at 77 K on all materials did not reveal any sorption hysteresis, whereas in the case of argon sorption at 87 K a small hysteresis loop could be detected for a pore diameter d_p,N$_2$(BJH): of ca. 2.8 nm (sample **C**), but not for pores smaller than 2.52 nm. For argon adsorption at 77 K ($T_R - T \approx 6.5$ K), pore condensation and hysteresis could be resolved for all MCM-48 materials studied here. The widths of hysteresis loops decrease with decreasing pore diameter, in accordance with the expectation that the fluid confined to the smaller pores of **A** may be closer to pore criticality as the fluid in the wider pores of **C**.

Argon sorption isotherms at 77 and 87 K in MCM-48 silica **C** show also that the width of the hysteresis loop decreases, as expected from theoretical predictions, for a given material with increasing temperature.[58] The difference in the occurrence of hysteresis for nitrogen and argon at 77 K can also be explained as a consequence of the lower reduced temperature T/T_c of argon compared to nitrogen, where T_c is the critical temperature of the bulk fluid (T/T_c(Ar) = 0.51; T/T_c(N$_2$) = 0.61). The observed argon sorption hysteresis loops in MCM-48 silica materials are of type H1, indicating that networking effects are not dominant for sorption hysteresis in the MCM-48 silicas studied here, despite the fact that MCM-48 consists of a unique three-dimensional pore network.

The occurrence of pore condensation and hysteresis in argon sorption isotherms at 77 K for MCM-48 with BJH pore diameter < 3 nm reveals that the (quasi) triple point of the pore fluid is shifted at least 6.5 K to lower temperature as compared with the triple-point temperature of the bulk fluid. In contrast, argon sorption isotherms at 77 K in the much wider pores of controlled-pore glass (BJH pore diameter ca. 16 nm) did not show any pore condensation and hysteresis, indicating that in such wide pores the pore condensation line does not extend down to this temperature for pressures up to the corresponding bulk sublimation pressure.

Phase transitions and pronounced sorption hysteresis of type H1 were also found for krypton sorption at 87 K in MCM 48 silica, i.e., ca 28.5 K below the bulk triple-point temperature. As in the case of argon sorption (77 K) it was found that the width of the hysteresis loop decreases with decreasing pore diameter, but is still observable for a BJH pore diameter as small as 2.1 nm. More work is necessary to explore details of the nature of the observed krypton phase transitions well below the bulk triple-point temperature.[103]

Acknowledgment. M.F. and R.K. acknowledge financial support by the Deutsche Forschungsgemeinschaft (Fr 1372/1-1, Fr 1372/2-1, Fr 1372/4-1) and the Fonds der Chemischen Industrie. M.T. acknowledges helpful discussions with Prof. G. H. Findenegg and thanks G. Scharschuh for technical support.

References and Notes

(1) Kresge, C. T.; Leonowicz, M. E.; Roth, W. J.; Vartuli J. C.; Beck, J. S. *Nature* **1992**, *359*, 710.

(2) Beck, J. S.; Vartuli, J. C.; Roth, W. J.; Leonowicz, M. E.; Kresge, C. T.; Schmitt, K. D.; Chu, C. T.-W.; Olson, D. H.; Sheppard, E. W.; McCullen, S. B.; Higgins J. B.; Schlenker, J. L. *J. Am. Chem. Soc.* **1992**, *114*, 10834.

(3) Corma, A. *Chem. Rev.* **1997**, *97*, 2373.

(4) Ying, J. Y.; Mehnert, C. P.; Wong, M. S. *Angew. Chem., Int. Ed. Engl.* **1999**, *38*, 56.

(5) Moller, K.; Bein, T. *Chem. Mater.* **1998**, *10*, 2950.

(6) Huo, Q.; Margolese, D. I.; Ciesla, U.; Demuth, D. G.; Feng, P.; Gier, T. E.; Sieger, P.; Firouzi, A.; Chmelka, B. F.; Schüth, F.; Stucky, G. D. *Chem. Mater.* **1994**, *6*, 1176.

(7) Tanev, P. T.; Pinnavaia, T. J. *Science* **1995**, *267*, 865.

(8) Bagshaw, S. A. Prouzet, E.; Pinnavaia, T. J. *Science* **1995**, *269*, 1242.

(9) Antonelli, D. M.; Nakahira, A.; Ying, J. Y. *Inorg. Chem.* **1996**, *35*, 3126.

(10) Fröba, M.; Tiemann, M. *Chem. Mater.* **1998**, *10*, 3475.

(11) Ciesla, U.; Schüth, F. *Microporous Mesoporous Mater.* **1999**, *27*, 131.

(12) Schmidt, R.; Stöcker, M.; Akporiaye, D.; Torstad, E. H.; Olsen, A. *Microporous Mater.* **1995**, *5*, 1.

(13) Alfredsson, V.; Anderson, M. W. *Chem. Mater.* **1996**, *8*, 1141.

(14) Alfredsson, V.; Anderson, M. W.; Ohsuna, T.; Terasaki, O.; Jacob, M.; Bojrup, M. *Chem. Mater.* **1997**, *9*, 2066.

(15) Auvray, X.; Petipas, C.; Anthore, R.; Rico, I.; Lattes, A. J. *J. Phys. Chem.* **1989**, *93*, 7458.

(16) Funari, S. S.; Rapp, *G. J. Phys. Chem. B* **1997**, *101*, 732.

(17) Monnier, A.; Schüth, F.; Huo, Q.; Kumar, D.; Margolese, D.; Maxwell, R. S.; Stucky, G. D.; Krishnamurty, M.; Petroff, P.; Firouzi, A.; Janicke, M.; Chmelka, B. F. *Science* **1993**, *261*, 1299.

(18) Stucky, G. D.; Monnier, A.; Schüth, F.; Huo, Q.; Margolese, D.; Kumar, D.; Krishnamurty, M.; Petroff, P.; Firouzi, A.; Janicke, M.; Chmelka, B. F. *Mol. Cryst. Liq. Cryst.* **1994**, *240*, 187.

(19) Vartuli, J. C.; Schmitt, K. D.; Kresge, C. T.; Roth, W. J.; Loenowicz, M. E.; McCullen, S. B.; Hellring, S. D.; Beck, J. S.; Schlenker, J. L.; Olson, D. H.; Sheppard, E. W. *Chem. Mater.* **1994**, *6*, 2317.

(20) Fyfe, C. A.; Fu, G. *J. Am. Chem. Soc.* **1995**, *117*, 9709.

(21) Huo, Q.; Margolese, D. I.; Stucky, G. D. *Chem. Mater.* **1996**, *8*, 1147.

(22) Zhang, W. Z.; Pinnavaia, T. J. *Catal. Lett.* **1996**, *38*, 261.

(23) Sayari, A. *Chem. Mater.* **1996**, *8*, 1840.

(24) Morey, M. S.; Davidson, A.; Stucky, G. D. *J. Porous Mater.* **1998**, *5,* 195.

(25) Morey, M.; Davidson, A.; Stucky, G. *Microporous Mater.* **1996**, *6*, 99.

(26) Koyano, K. A.; Tatsumi, T. *Chem. Commun.* **1996**, 145.

(27) Corma, A.; Kan, Q.; Rey, F. *Chem. Commun.* **1998**, 579.

(28) Ahn, W. S.; Lee, D. H.; Kim, T. J.; Kim, J. H.; Seo, G.; Ryoo, R. *Appl. Catal. A* **1999**, *181*, 39.

(29) Anpo, M.; Yamashita, H.; Ikeue, K.; Fujii, Y.; Zhang, S. G.; Ichihashi, Y.; Park, D. R.; Suzuki, Y.; Koyano, K.; Tatsumi, T. *Catal. Today* **1998**, *44*, 327.

(30) Walker, J. V.; Morey, M.; Cralsson, H.; Davidson, A.; Stucky, G. D.; Butler, A. *J. Am. Chem. Soc.* **1997**, *119*, 6921.

(31) Morey, M.; Davidson, A.; Eckert, H.; Stucky, G. *Chem. Mater.* **1996**, *8*, 486.

(32) VanDerVoort, P.; Morey, M.; Stucky, G. D.; Mathieu, M.; Vansant, E. F. *J. Phys. Chem. B* **1998**, *102*, 585.

(33) Kawi, S.; Te, M. *Catal. Today* **1998**, *44*, 101.

(34) Zhao, D. Y.; Goldfarb, D. *J. Chem. Soc., Chem. Commun.* **1995**, 875.

(35) Kosslick, H.; Lischke, G.; Landmesser, H.; Parlitz, B.; Storek, W.; Fricke, R. *J. Catal.* **1998**, *176*, 102.

(36) Schmidt, R.; Junggreen, H.; Stocker, M. *Chem. Commun.* **1996**, 875.

(37) Romero, A. A.; Alba, M. D.; Klinowski, J. *J. Phys. Chem. B* **1998**, *102*, 123.

(38) Echchahed, B.; Moen, A.; Nicholson, D.; Bonneviot, M. *Chem. Mater.* **1997**, *9,* 1716.

(39) Hartmann, M.; Racouchot, S.; Bischof, C. *Chem. Commun.* **1997**, 2367.

(40) Reller, A.; Ebbinghaus, S.; Köhn, R.; Fröba, M.; Sazama, U.; Fortunato, P. *Mater. Res. Soc. Symp. Proc.* **1999**, *547*, 75.

(41) Morey, M.; Stucky, G. D.; Schwarz, S.; Fröba, M. *J. Phys. Chem. B* **1999**, *103*, 2037.

(42) Fröba, M.; Köhn, R.; Bouffaud, G.; Richard, O.; Van Tendeloo, G. *Chem. Mater.* **1999**, *11*, 2858.

(43) Romero, A. A.; Alba, M. D.; Zhou, W.; Klinowski, J. *J. Phys. Chem. B* **1997**, *101*, 5294.

(44) Behrens, P.; Glaue, A.; Haggenmüller, Ch.; Schechner, G. *Solid State Ionics* **1997**, *101*−*103*, 255.

(45) Xu, J.; Luan, Z.; He, H.; Zhou, W.; Kevan, L. *Chem. Mater.* **1998**, *10*, 3690.

(46) Van der Voort, P.; Mathieu, M.; Mees, F.; Vansant, E. F. *J. Phys. Chem. B* **1998**, *102*, 8847.

(47) Chen, F.; Huang, L.; Li, Q. *Chem. Mater.* **1997**, *9*, 2685.

(48) Kim, J. M.; Kim, S. K.; Ryoo, R. *Chem. Commun.* **1998**, 259.

(49) Schumacher, K.; Grün, M.; Unger, K. K. *Microporous Mesoporous Mater.* **1999**, *27*, 201.

(50) Schulz-Ekloff, G.; Rathousky, J.; Zukal, A. *Microporous Mesoporous Mater.* **1999**, *27*, 273.

(51) Gallis, K. W.; Landry, C. C. *Chem. Mater.* **1997**, *9*, 2035.

(52) Ryoo, R.; Joo, S. H.; Kim, J. M. *J. Phys. Chem. B* **1999**, *103*, 7435.

(53) Hartmann, M.; Bischof, C.; *J. Phys. Chem. B* **1999**, *103*, 6230.

(54) Gregg, S. J.; Sing, K. S. W. *Adsorption, Surface Area and Porosity*; Academic Press: London, 1982.

(55) Rouquerol, F.; Roquerol, J.; Sing, K. S. W. *Adsorption by Powders & Porous Solids*; Academic Press: London, 1999.

(56) Sing, K. S. W.; Everett, D. H.; Haul, R. A. W.; Mouscou, L.; Pierotti, R. A.; Rouquerol, J.; Siemieniewska, T. *Pure Appl. Chem.* **1985**, *57*, 603.

(57) Everett, D. H. In *The Solid*−*Gas Interface*; Flood, E. A., Ed.; Marcel Dekker: New York, 1967; Vol. 2.

(58) Ball, P. C.; Evans, R. *Langmuir* **1989**, *5*, 714.

(59) Page, J. H.; Liu, J.; Abeles, B.; Herbolzheimer, E.; Deckmann, W. A.; Weitz, D. A. *Phys. Rev. E* **1995**, 52, 2763.

(60) Cole, M. W.; Saam, W. F. *Phys. Rev. Lett.* **1974**, *32*, 985.

(61) Awschalom, D. D.; Warnock, J.; Shafer, M. W. *Phys. Rev. Lett.* **1996**, *57*, 1607.

(62) Findenegg, G. H.; Gross, S.; Michalski, T. In *Characterization of porous solids III. Studies in Surface Science and Catalysis* 87; Roquerol, J., Rodriguez-Reinoso, F., Sing, K. S. W., Unger, K. K., Eds.; Elsevier: Amsterdam, 1994.

(63) Papadopolou, A.; van Swol, F.; Marconi, U. M. B. *J. Chem. Phys.* **1992**, *97*, 6942.

(64) Mason, G. *J. Colloid Interface Sci.* **1982**, *88*, 36.

(65) Mason, G. *J. Colloid Interface Sci.* **1983**, *95*, 277.

(66) Neimark, A. V. *Russian J. Phys. Chem.* **1986**, *60*, 1045.

(67) Liu, H.; Zhang, L.; Seaton, N. A. *Langmuir* **1993**, *9*, 2576.

(68) Liu, H.; Seaton, N. *Chem. Eng. Sci.* **1994**, *49*, 1869.

(69) Lastoskie, C. M.; Gubbins, K.; Quirke, N. *J. Phys. Chem.* **1993**, *97*, 4786.

(70) Tarazona, P.; Marconi, U. M. B.; Evans, R. *Mol. Phys.* **1987**, *60*, 543.

(71) Evans, R. *J. Phys. Condens. Matter* **1990**, *2*, 8989.

(72) Binder, K.; Landau, D. P *J. Chem. Phys.* **1992**, *96*, 1444.

(73) Walton, J. P. R. P.; Quirke, N. *Mol. Simul.* **1989**, *2*, 361.

(74) Gubbins, K. E. In *Physical Adsorption: Experiment, Theory and Applications*, Fraissard, J., Ed.; Kluwer: Dordrecht, 1997.

(75) Fisher, M. E.; Nakanishi, H. *J. Chem. Phys.* **1981**, *75*, 5857.

(76) Tovbin, Y. K.; Votyakov, E. V. *Langmuir* **1993**, *9*, 2652.

(77) Eyrad, C.; Brun, M.; Eyraud, L.; Lallemand, A.; Eyraud, P. *C. R. Acad. Sci. Paris* **1971**, *273 (B)*, 645.

(78) Fretwell, H. M.; Duffy, J. A.; Clarke, A. P.; Alam, M. A.; Evans, R. *J. Phys.: Condens. Matter* **1996**, *8*, 9613.

(79) Dominguez, H.; Allen, M. P.; Evans, R. *Mol. Phys.* **1998**, *96*, 209.

(80) Thommes, M.; Findenegg, G. H. *Langmuir* **1994**, *10*, 4270.

(81) Findenegg, G. H.; Thommes, M. In *Physical Adsorption: Experiment, Theory and Applications*; Fraissard, J.; Ed.; Kluwer: Dordrecht, 1997.

(82) Gelb, L. D.; Gubbins, K. E.; Radhakrishnan, R.; Sliwinska-Bartkowiak, M. *Rep. Prog. Phys.* **1999**, 62, 1573

(83) Branton, P. J.; Hall, P. G.; Sing, K. S. W. *J. Chem. Soc., Chem. Commun.* **1993**, 1257.

(84) Franke, O.; Schulz-Ekloff, G.; Rathousky, J.; Starek, J.; Zukal, A. *J. Chem. Soc., Chem. Commun.* **1993**, 724.

(85) Morishige, K.; Fujii, H.; Uga, M.; Kinukawa, D. Lan*gmuir* **1997**, *13*, 3948.

(86) Kruk, M.; Jaroniec, M.; Sayari, A. *J. Phys. Chem. B* **1997**, *101*, 583.

(87) Rathousky, J.; Zukal, A.; Franke, O.; Schulz-Ekloff, G. *J. Chem. Soc., Faraday Trans.* **1994**, *90*, 2821.

(88) Schmidt, R.; Stöcker, M.; Hansen, E.; Akporiaye, D.; Ellestad, O. H. *Microporous Mater.* **1995**, *3*, 443.

(89) Ravikovitch, P. I.; Domhnaill, S. C. O.; Neimark, A. V.; Schüth, F.; Unger, K. K. *Langmuir* **1995**, *11*, 4765.

(90) Ravikovitch, P.; Wie, D.; Church, W. T.; Haller, G. L.; Neimark, A. W. *J. Phys. Chem. B* **1997**, *101*, 3671.

(91) Neimark, A. V.; Ravikovitch, P. I.; Grün, M.; Schüth, F.; Unger, K. K. *J. Colloid Interface Sci.* **1998** *207*, 159.

(92) Sonwane, C. G.; Bathia, S. K.; Calos, N. *Ind. Eng. Chem. Res.* **1998**, *37*, 2271.

(93) Barrett, E. P.; Joyner, L. G.; Halenda, P. P. *J. Am. Chem. Soc.* **1951**, *73*, 373.

(94) Saito, A.; Foley, H. C. *AIChE J.* **1991**, *37*, 429.

(95) Saito, A.; Foley, H. C. *Microporous Mater.* **1995**, *3*, 531.

(96) Horvath, G.; Kawazoe, K. *J. Chem. Eng. Jpn.* **1983**, *16*, 474.

(97) Galarneau, A.; Desplantier, D.; Dutartre, R.; Di Renzo, F. *Microporous Mesoporous Mater.* **1999**, *27*, 297.
(98) Lastoskie, C. M.; Gubbins, K. E. In *Characterization of Porous Solids, V. Studies in Surface Science and Catalysis 128*; Unger K. K., Kreysa G., Baselt P., Eds.; Elsevier: Amsterdam, 2000.
(99) Nguyen, C.; Do, D. D. *Langmuir* **1999**, *15*, 3608.
(100) Inoue, S.; Hanzawa, Y.; Kaneko, K. *Langmuir* **1998**, *14*, 3079.
(101) Maddox, M. W.; Olivier, J. P.; Gubbins, K. E. *Langmuir* **1997**, *13*, 1737.
(102) Gross, S.; Findenegg, G. H. *Ber. Bunsen-Ges. Phys. Chem.* **1997**, *101*, 1726.
(103) Thommes, M.; Köhn, R.; Fröba, M. **2000**. To be published.
(104) Coulomb, J. P.; Grillet, Y.; Llewellyn, P. L.; Martin, C.; Andre, G. In *Fundamentals of Adsorption*; Meunier, F., Ed.; Elsevier: Paris, 1998.
(105) Rabinovich, V. A.; Vasserman, A. A.; Neodostup, V. I.; Veksler, L. S. *Thermophysical Properties of Neon, Argon, Krypton, and Xenon*; Hemisphere Publishing: Washington, DC, 1988.
(106) Burgess, C. G. V.; Everett, D. H.; Nuttall, S. *Pure Appl. Chem.* **1989**, *61*, 1845.
(107) Lide, D. R., Ed. *Handbook of Chemistry and Physics*, 79th ed.; CRC Press: Washington, 1998.